Plasmonics (2015) 10:419–427
DOI 10.1007/s11468-014-9823-z

# Impact of a Dielectric Layer on the Resonant Conditions of Nanograting Structures

**Chao Niu · Tiffany Huang · Xin Zhang · Haitao Liu · Weihua Zhang · Jonathan Hu**

Received: 24 July 2014 / Accepted: 2 November 2014 / Published online: 23 November 2014


**Abstract** We study the resonant wavelength of nanograting structures covered by a dielectric medium. We find that the resonant wavelength oscillates as the thickness of the thin dielectric layer increases due to the cavity formed by the dielectric layer. The amplitude of this oscillation in the resonant wavelength is small when the minimum reflection occurs in the nanograting structure. For a plasmonic sensor covered by a dielectric medium, a small oscillation in the resonant wavelength as the thickness of the dielectric medium changes is preferred. We also study the impact of a rounded corner on the resonant wavelength and find that the rounded corners with a small radius of $r$ effectively reduce the nanogroove depth by about $0.2r$. Results from the finite-difference time-domain (FDTD) method agree very well with the phase-matching condition, using parameters calculated from the rigorous coupled-wave analysis (RCWA) method. These results will lead to a better understanding of the accuracy of plasmonic sensors covered by dielectric media.

C. Niu · T. Huang · J. Hu (✉)
Department of Electrical and Computer Engineering,
Baylor University, Waco, TX 76798, USA
e-mail: jonathan_hu@baylor.edu

C. Niu
e-mail: chao_niu@baylor.edu

X. Zhang · H. Liu
Key Laboratory of Optical Information Science and Technology,
Ministry of Education, Institute of Modern Optics,
Nankai University, Tianjin 300071, China

W. Zhang
College of Engineering and Applied Sciences, Nanjing University,
Nanjing 210093, China

**Keywords** Nanostructures · Metallic grating · Surface plasmons · Sensors

## Introduction

Surface plasmons are charge density oscillations that exist at the interface of two materials, which have dielectric constants of opposite signs, such as a metal and a dielectric medium [1]. Surface plasmon resonances are of particular interest because of the high optical field confinement at the resonant wavelengths. When a metal surface is in contact with a dielectric medium, the resonant wavelengths for surface plasmon waves are very sensitive to the refractive index of the dielectric medium [2–4]. By studying the resonant wavelength, one is able to determine the refractive index of a dielectric medium on top of a plasmonic structure. Hence, plasmonic sensor devices can be used in the next generation of biosensors for fast, real-time identification of biomarkers in new health-care programs [5–8]. Many successful sensors have been implemented in biosensor applications using the resonant wavelength [9–20]. Significant progress has been made using the resonant wavelengths of different metal structures. However, a detailed analysis of dielectric layer thickness, which may have a strong impact on the resonant wavelength [21], has not been thoroughly conducted. Measurements may be inaccurate due to variations in the thickness of the dielectric layer. The interaction between fields in the dielectric layer and fields at the metal surface will impact the resonant wavelength of a sensor device. These phenomena may potentially decrease the accuracy of a plasmonic sensor.

In this paper, we analyze simple and commonly used plasmonic nanograting structures covered by a dielectric

layer. Nanograting structures have been shown to have a high enhancement factor on electromagnetic fields at the resonant wavelength [17–20]. We first use the finite-difference time-domain (FDTD) method to study resonant wavelengths of nanograting structures. We find that resonant wavelengths determined using the FDTD method agree very well with the phase-matching condition, using coefficients calculated with the rigorous coupled-wave analysis (RCWA) method [22–24]. Then, we study the resonant wavelength of a nanograting structure covered by a thin dielectric layer. We find that, because of the cavity formed in the dielectric layer, the resonant wavelength oscillates with the increase of the thickness of the dielectric medium. For a plasmonic sensor covered by a dielectric medium, a small oscillation in the resonant wavelength as the thickness of the dielectric medium changes is preferred. This reduces measurement error due to uncertainty of the thickness of the dielectric medium. We also study the impact of a rounded corner in the nanograting structure on the resonant wavelength. We determine that the rounded corners with a small radius of $r$ effectively reduce the nanogroove depth by about $0.2r$. These results will lead to a better understanding of the accuracy of plasmonic sensor devices covered by dielectric media. The results may be generalized to other types of plasmonic devices.

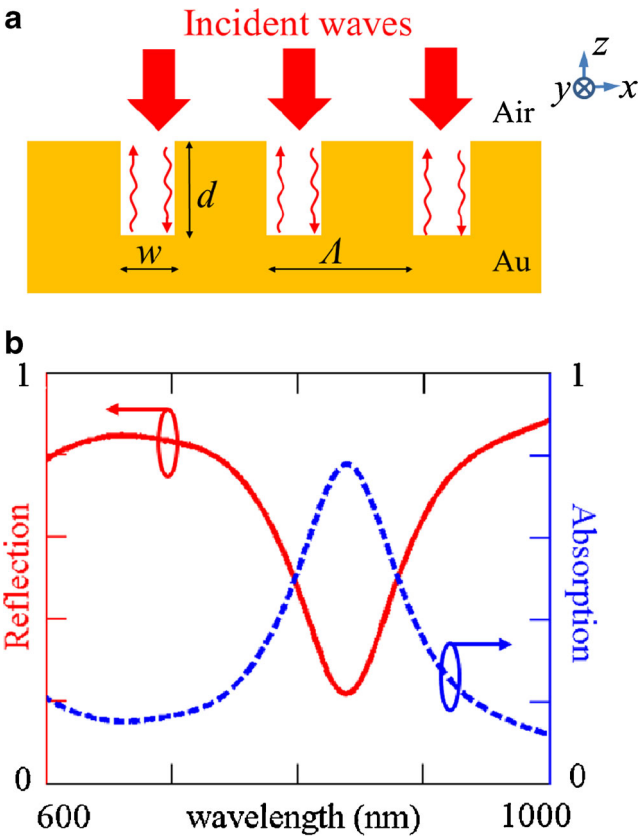


**Fig. 1** **a** Schematic illustration of nanograting. **b** Reflection and absorption when $w = 60$ nm, $d = 90$ nm, and $\Lambda = 560$ nm

## Structures and Modeling

In this paper, we consider a nanograting structure, as shown in Fig. 1a. The nanograting period, nanogroove width, and nanogroove depth are denoted as $\Lambda$, $w$, and $d$, respectively. The nanograting structure is infinitely long and invariant in the $y$-direction. In the simulation, we use the FDTD solver from Lumerical to calculate light scattering in the nanograting structure. The simulation uses experimentally measured refractive indices of gold [25]. The refractive index of air is 1. The incident plane wave propagates from the top of the device with transverse magnetic (TM) polarization (magnetic vector along the invariant $y$-direction). We use periodic boundary condition on the boundaries in positive and negative $x$-directions. The reflection monitor is located behind the light source to collect all the reflected light. Figure 1b shows reflection, $R$, and absorption, $A$, on the nanograting structure, with $w = 60$ nm, $d = 90$ nm, and $\Lambda = 560$ nm. The same nanograting parameters as in [26] are used here. We set $A = 1 - R$, with a thick Au nanostructure substrate. The incident plane waves excite the surface plasmonic waves at the interface between air and the Au nanograting structure. We determine that the resonant wavelength for this structure is approximately 840 nm, as shown in Fig. 1b. Resonance occurs when the localized surface plasmon modes in nanogrooves satisfy the phase-matching condition [27]:

$$2k_0\mathrm{Re}(n_{\mathrm{eff}})d + \arg(r_a) + \arg(r_m) = 2m\pi, \quad (1)$$

where $r_a$ and $r_m$ are reflection coefficients of the fundamental surface plasmon modes at the upper and lower ends of the nanogroove array, respectively, as shown in Fig. 2a. We use RCWA to calculate the reflection coefficients $r_a$ and $r_m$ as functions of wavelength and nanogroove width, as shown in Fig. 2b, c, respectively. The function $\arg(x)$ represents the argument or phase of a complex number $x$. In Fig. 2b, with a narrower groove width, the fields are mainly located near the nanogroove and the structure yields smaller phase delays for the reflection coefficient, $r_a$, at the upper end of the groove. The reflection coefficient at the metal end of the groove, $r_m$, stays almost the same. Note the $\pi$ phase shift is included in the reflection from the metal surface. In Fig. 2c, as the wavelength increases, the relative width becomes narrow, which yields less phase delay on the long wavelength side. The value, $m$, is a positive integer in Eq. 1. The value, $n_{\mathrm{eff}}$, represents the effective index of the surface plasmon fundamental mode in the nanogrooves.

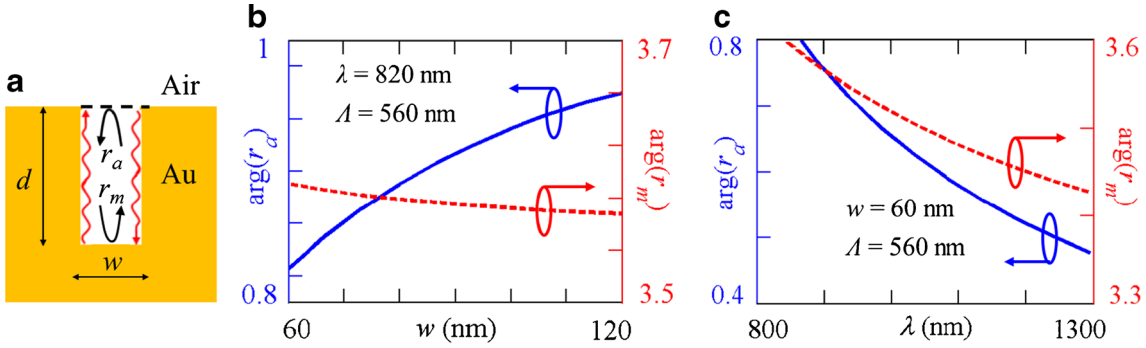


**Fig. 2** **a** Schematic of the reflection coefficients, $r_a$ and $r_m$. Phase delay of $r_a$ and $r_m$ for **b** different groove widths and **c** different wavelengths

This surface plasmon mode in the nanogroove structure can be approximated by the mode in a metal-insulator-metal (MIM) structure with an infinitely long nanograting depth and pitch. The characteristic equation for the MIM structure is, $\tanh(k_i w/2) = -\epsilon_i k_m/(\epsilon_m k_i)$, where $w$ is the insulator width [28, 29]. The wave vectors in the air and metal, perpendicular to the interfaces, $k_i$ and $k_m$, are defined as $k_i = (\beta^2 - k_0^2\epsilon_i)^{1/2}$ and $k_m = (\beta^2 - k_0^2\epsilon_m)^{1/2}$, respectively. Note that $\beta$, $\epsilon_i$, and $\epsilon_m$ are the propagation constant, permittivity of insulator, and permittivity of metal, respectively. Figure 3 shows the real part of the effective index, $\mathrm{Re}(n_{\mathrm{eff}}) = \mathrm{Re}(\beta)/k_0$, as a function of wavelength and nanogroove width. Note that $k_0 = 2\pi/\lambda$ is the wave number in vacuum.

With the parameters for the nanograting structure, we are able to calculate the resonant wavelength to satisfy the phase-matching condition. In Fig. 4, solid lines show resonant wavelength as a function of nanogroove width and depth, derived using FDTD simulations. We can see that resonant wavelength increases as nanogroove depth increases [30]. However, resonant wavelength does not change much when the nanogroove width changes. To confirm the results of FDTD simulations in Fig. 4, we calculate resonant wavelength as a function of groove width indicated by blue circles, using the phase-matching condition in Eq. 1. Reflection coefficients are calculated by the RCWA method as shown in Fig. 2. Note that nanogroove width does not directly exist in Eq. 1. The increase in nanogroove width from 60 to 120 nm only indirectly leads to a decrease in the $n_{\mathrm{eff}}$ from 1.42 to 1.22, as shown in Fig. 3b. Hence, resonant wavelength slightly decreases when the nanogroove width increases and $n_{\mathrm{eff}}$ decreases according to the phase-matching condition in Eq. 1. To determine values marked by red circles, we calculate $n_{\mathrm{eff}}$, $r_a$, and $r_m$ as a function of the resonant wavelength. Then, depth, $d$, can be determined using Eq. 1, shown as red circles in Fig. 4. Alternatively, one could use depth, $d$, to determine the resonant wavelength, assuming $n_{\mathrm{eff}}$, $r_a$, and $r_m$ are wavelength-independent parameters. However, this will result in an approximate 10 % error in the resonant wavelength because $n_{\mathrm{eff}}$, $r_a$, and $r_m$ vary with the resonant wavelength. We use a pitch of 560 nm for the Fig. 4. If pitch changes, the resonant wavelength varies as $r_a$ and $r_m$ vary with pitch.

## Thickness of the Dielectric Layer

Now, we study a nanograting structure covered by a dielectric medium, such as liquid, as shown in Fig. 5. The nanograting period, nanogroove width, and nanogroove depth are denoted as $\Lambda$, $w$, and $d$, respectively. The thickness of the dielectric medium, $t$, is defined as the distance

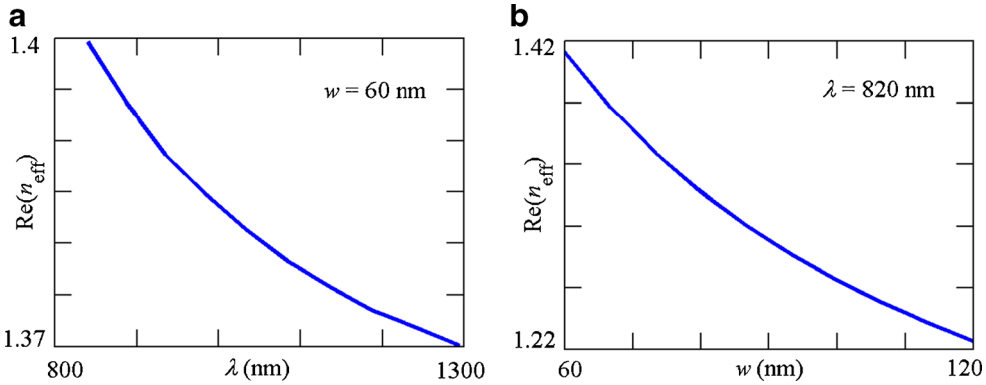


**Fig. 3** **a** The real part of the effective index, $n_{\mathrm{eff}}$, as a function of λ. **b** The real part of the effective index, $n_{\mathrm{eff}}$, as a function of nanogroove width

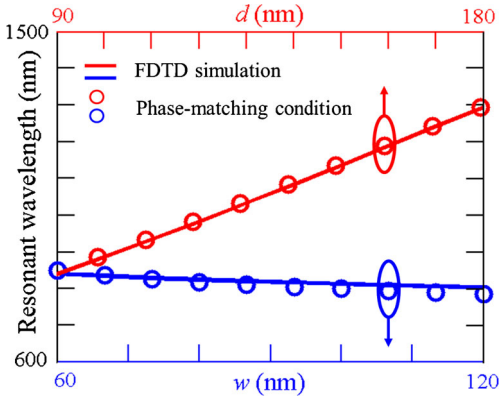


**Fig. 4** Comparison of simulation results from FDTD and phase-matching condition

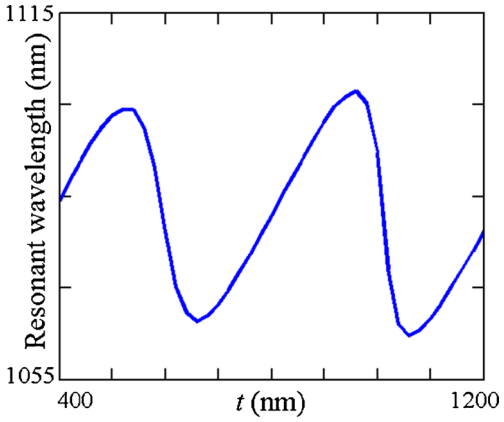


**Fig. 6** Resonant wavelength versus $t$ when $\Lambda = 560$ nm, $w = 60$ nm, and $d = 90$ nm

between the top of the dielectric medium and the top of the nanogroove. Figure 6 shows resonant wavelengths for different thicknesses of dielectric medium on top of the nanogrooves with $w = 60$ nm, $d = 90$ nm, and $\Lambda = 560$ nm. We use liquid as an example, with a refractive index of $n = 1.3$ [30]. When the liquid thickness increases from 400 to 1200 nm, resonant wavelength oscillates between 1060 and 1110 nm, as shown in Fig. 6. We can see that the amplitude of oscillation is approximately 40 nm. Figure 7a shows the reflection curves as the liquid thickness increases. The blue solid curve shows the reflection curve with a liquid thickness of 806 nm and a resonant wavelength of 1080 nm. The purple dashed curve shows the reflection curve with a larger liquid thickness of 939 nm and a slightly longer resonant wavelength of 1105 nm. The reason is that the dielectric layer forms a cavity. At the top of the cavity, the waves are partly reflected from the interface between liquid and air. At the bottom of the cavity, the waves are partly reflected from the interface between liquid and Au top surface. A slightly thicker cavity leads to a slightly longer resonant wavelength. On the other hand, a reduced liquid thickness of 666 nm leads to a slightly shorter resonant wavelength of 1060 nm, as indicated by the solid purple curve. When liquid thickness is 1009 nm, waves in the cavity destructively interfere with each other and the resonant wavelength comes back to 1080 nm. Hence, as liquid thickness changes, the resonant wavelengths are bound by

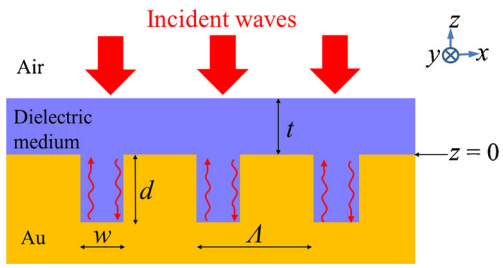


**Fig. 5** Schematic of nanograting structure covered by a dielectric medium

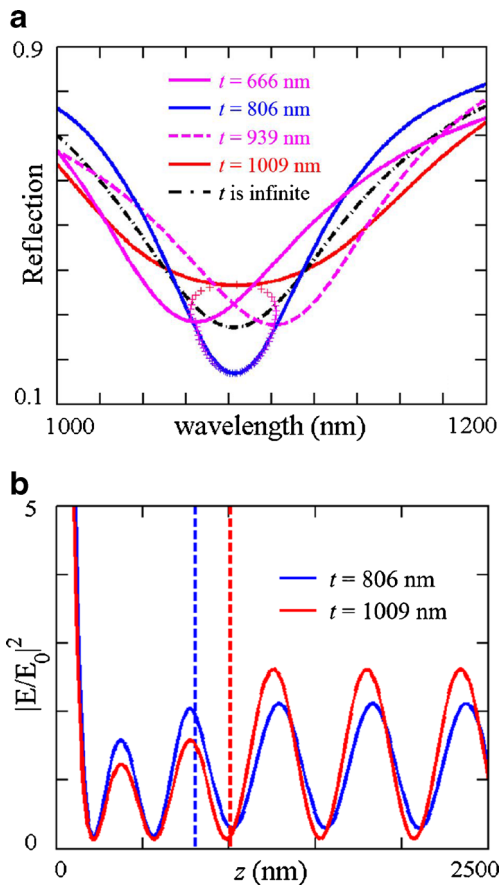


**Fig. 7** **a** Reflection versus wavelength when $t$ changes with $\Lambda = 560$ nm, $w = 60$ nm, and $d = 90$ nm. The resonant wavelengths are bound by the plus signs as $t$ changes. **b** Normalized $|\mathbf{E}/\mathbf{E}_0|^2$ along $z$-axis both inside and above the liquid at $x = 0$. Blue and red dashed lines indicate the locations of $t = 806$ and 1009 nm, respectively

the plus signs in Fig. 7a. We also show the reflection curve for liquid of infinite thickness with no cavity effect as the black dash-dotted curve. Note that the minimum point of the black dash-dotted curve locates at the center of the plus signs, which confirms that the resonant wavelength for a nanograting structure without cavity effect is 1080 nm.

Figure 7b shows the electric field profile both inside and above the liquid at the resonant wavelength when liquid thicknesses are 806 and 1009 nm, corresponding to the cases of constructive interference and destructive interference, respectively, for the waves inside the cavity of the dielectric layer. The electric field magnitude is larger for the blue curve inside the cavity when the liquid thickness is 806 nm. The waves experience constructive interference inside the dielectric cavity, which indicates the phase delay in one round trip inside the cavity is $2\pi$ or a multiple of $2\pi$. With a slightly stronger field inside the dielectric layer, additional absorption occurs at the metal surface, leading to a slightly weaker field above the dielectric layer ($z > 806$ nm) in the air. On the other hand, the case with liquid thickness of 1009 nm has a reduced field amplitude inside the dielectric cavity because waves experience destructive interference. Note that the difference in electric fields between the cases with the thicknesses of 806 and 1009 nm is not very large due to a small difference in the refractive indices of liquid and air. However, this small cavity effect causes oscillations in the resonant wavelength, as shown in Fig. 6. The large field magnitude near $z = 0$, comes from the high plasmonic field concentration near the corner of the nanograting structure [26].

We also study the variation in the resonant wavelength, $\Delta\lambda$, which is defined as the maximum variation in resonant wavelength between liquid thickness of 400 and 1200 nm. For example, the variation in resonant wavelength, $\Delta\lambda$, is about 40 nm in Fig. 6. Figure 8a and b show the contour plots for variation in resonant wavelength, $\Delta\lambda$. We find that the variation is less than 5 nm, with a large pitch of 1000 nm, a small nanogroove width of 60 nm, and a small nanogroove depth of 90 nm. A small variation occurs with a large pitch, a small nanogroove width, and a small nanogroove depth for a small reflection, as shown in Fig. 8c, d. When the reflection is small, most of the power is absorbed by the nanogroove. The cavity effect has little impact on the resonant wavelength. We use liquid as an example for thin dielectric layer, with a refractive index of 1.3, for the contour plots in Fig. 8. Our analysis can be generalized to other thin dielectric media with different refractive indices. We also try a different refractive index of 1.35 and obtain results similar to the results shown in Fig. 8.

## Sensitivity and Figure of Merit

Next, we study the resonant wavelength when the refractive index of the liquid changes. Figure 9a shows results using

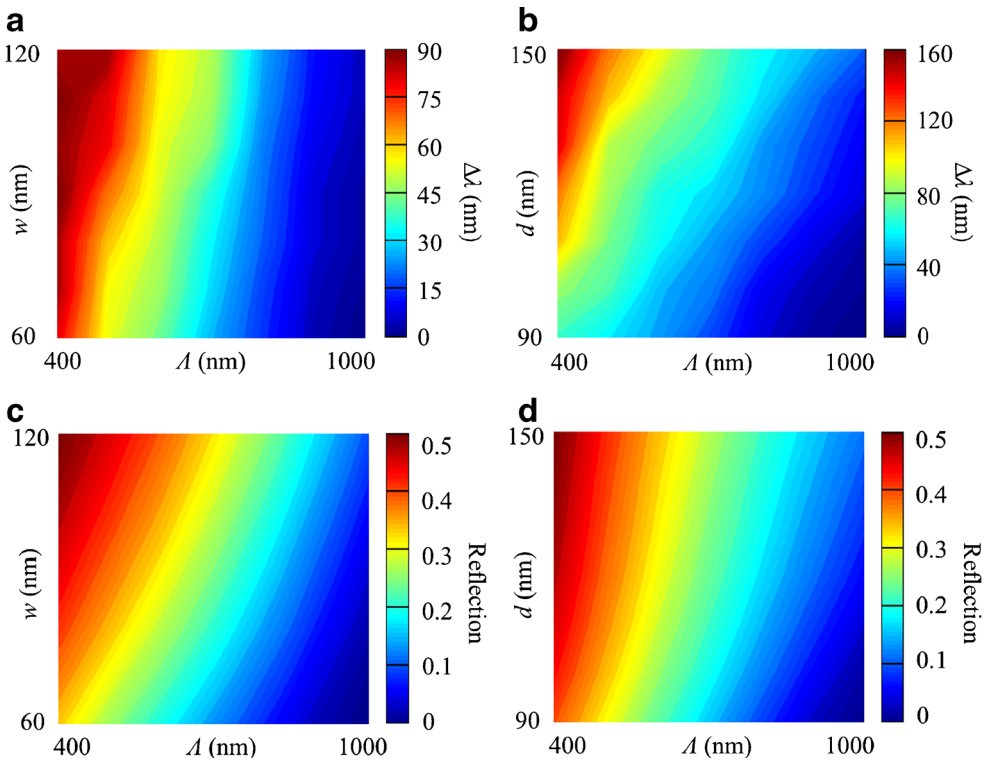


**Fig. 8** **a** Contour plot of $\Delta\lambda$ vs. pitch and width. **b** Contour plot of $\Delta\lambda$ vs. pitch and depth. **c** Contour plot of reflection vs. pitch and width. **d** Contour plot of reflection vs. pitch and depth

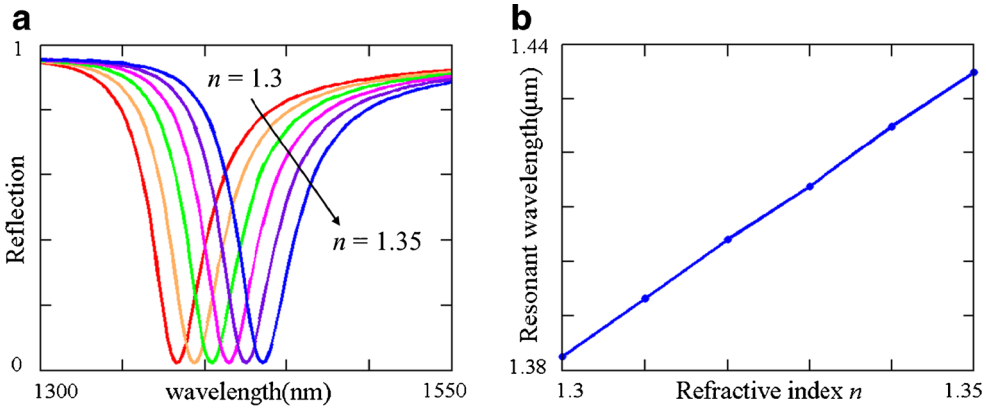


**Fig. 9** **a** Resonant wavelength changes as refractive index changes. **b** The resonant wavelength as a function of refractive index when $\Lambda = 1000$ nm, $w = 60$ nm, $d = 90$ nm, and $t = 800$ nm

the nanograting structure with $\Lambda = 1000$ nm, $w = 60$ nm, $d = 90$ nm, and $t = 800$ nm. Resonant wavelength varies from 1382 to 1435 nm, corresponding to the variations of the refractive index from 1.3 to 1.35. Hence, the refractive index of the dielectric medium can be determined by the resonant wavelength. Sensitivity, which is defined as the ratio of the change in wavelength to the change in refractive index unit (RIU), $S = \Delta\lambda/\Delta n$ , is approximately 1050 nm/RIU, as shown in Fig. 9b. When a plasmonic sensor is covered by a dielectric medium, such as liquid, the thickness of the liquid might not be determined accurately. Hence, small variations in resonant wavelength would be preferred with changes in thickness of the dielectric medium. In this case, variations in thickness of the liquid will lead to a maximum change of 5 nm in resonant wavelength according to Fig. 8, which may cause a maximum error in estimation of a refractive index of 0.005. Note that previously reported sensors had sensitivities of 235 nm/RIU in a nanoparticle sensor [31], 400 nm/RIU in a circular nanohole arrays sensor [32] and infrared perfect absorber [33], 450 nm/RIU in nanohole arrays [34], 600 nm/RIU in a double-hole arrays sensor [35] and nanobar array plasmonic sensor [36], 1015 nm/RIU mushroom arrays [37], 1110 nm/RIU in a two-dimensional nanohole array sensor [38], and 1190 nm/RIU in an array of split ring resonators [39].

The figure of merit (FOM) is often used to evaluate the overall performance of the plasmonic sensors. FOM is defined as the ratio of sensitivity to full-wave half-maximum (FWHM) of the reflection curve, $S$/FWHM [36, 40, 41]. Figure 10 shows contour plots of the FOM as a function of nanogroove width, $w$, nanogroove depth, $d$, and nanogroove pitch, $\Lambda$. From the contour plots, we can see that FOM is larger with a larger pitch, a smaller nanogroove width, and a smaller nanogroove depth. We use reflection curves in Fig. 11 to explain the FOM in Fig. 10. As pitch increases, FWHM decreases and FOM increases as shown in Fig. 11a. The momentum conservation for the coupling of surface plasmons on the metal-dielectric surface requires $m \cdot k_g = k_{sp}$, where $k_g$ is defined as $2\pi/\Lambda$, $k_{sp} = k_0[\epsilon_i\epsilon_m/(\epsilon_i + \epsilon_m)]^{1/2}$ is the propagation constant for the surface plasmon wave, and $m$ is a positive integer [26, 27]. Simple calculation for momentum conservation shows that $\Lambda$ is approximately 1000 nm for a wavelength of 1300 nm, which indicates that strong resonance occurs with a larger $\Lambda$ approaching 1000 nm. Figure 11b shows that FWHM decreases and FOM increases as width, $w$, decreases. The structure with a small width yields strong field and a strong resonance, which leads to a small FWHM and a large FOM [36, 42]. Note that the change in resonant wavelength is about 40 nm, when the width changes from 60 to 120 nm.

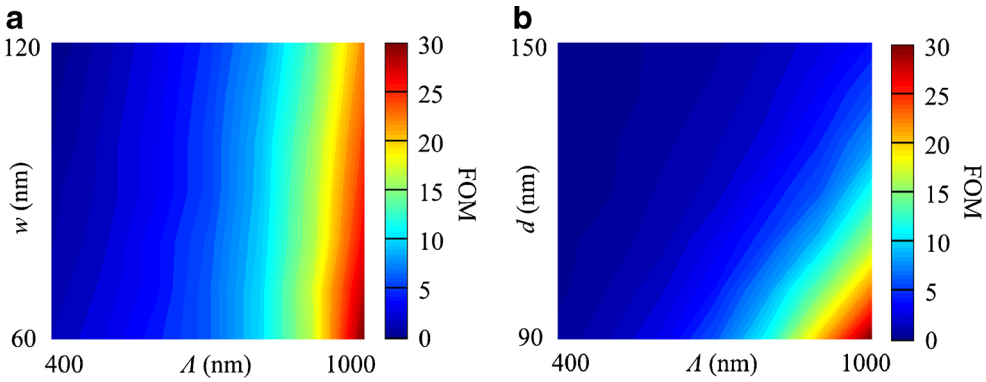


**Fig. 10** **a** Contour plot of FOM when $d = 90$ nm. **b** Contour plot of FOM when $w = 60$ nm

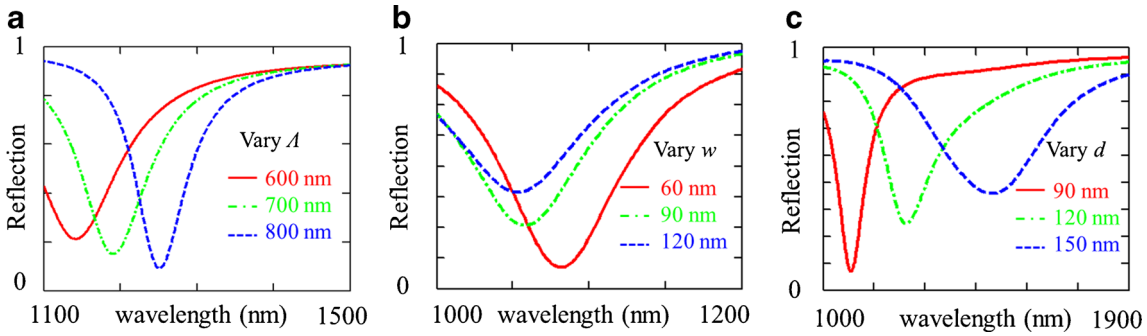


**Fig. 11** **a** Reflection with different $\Lambda$ when $d = 90$ nm and $w = 60$ nm. **b** Reflection with different $w$ when $\Lambda = 560$ nm and $d = 90$ nm. **c** Reflection with different $d$ when $\Lambda = 560$ nm and $w = 60$ nm

This amount of change is consistent with the amount of change shown in Fig. 4. Figure 11c shows that FWHM decreases and FOM increases as depth, $d$, decreases. The reason is that the short depth in nanogroove leads to a low propagation loss in surface plasmon waves and a strong resonance, which leads to a small FWHM and a large FOM [43]. Note that the change of FOM is mainly dominated by the relative change of FWHM in the parameter range considered here. The relative change in sensitivity, $S$, is only about 20 % of the relative change in the FWHM.

## The Rounded Corners in Nanogrooves

During the fabrication process, nanograting corners cannot be extremely sharp. In this part of analysis, we study the impact of rounded corners on resonant wavelength in nanograting structures. Figure 12a shows reflection curves as a function of wavelength for different radii of the rounded corners, as shown in inset. The thickness of the liquid is 800 nm. As the radii of the rounded corners increase, the resonant wavelength decreases. This is caused by effective reduction in the depth of the nanogroove. Figure 12b shows resonant wavelength as a function of radii of the rounded corners, $r$, as red circles. The solid line shows the linear regression fit, $\lambda = \lambda_0 - Ar$, where $\lambda_0 = 1080$ nm is the resonant wavelength with an extremely sharp corner ($r = 0$) and $A = 2$ is the fitting slope. Hence, rounded corners with a small radius of $r$ will lead to a shift in the resonant wavelength of nearly twice the radius, $2r$. We also compare the slope in Fig. 12b with the ratio of the change in resonant wavelength to the change in nanogroove depth as shown in Fig. 11c. The rounded corners with a small radius of $r$ effectively reduce the nanogroove depth by about $0.2r$, taking into account the rounded corners in both top and bottom of the nanogroove.

## Conclusion

We show the analysis of the resonant conditions for nanograting structures. Simulation data from FDTD agrees well with the phase-matching condition, using the reflection coefficients calculated from RCWA. We also study the impact of a thin dielectric medium above the nanogrooves

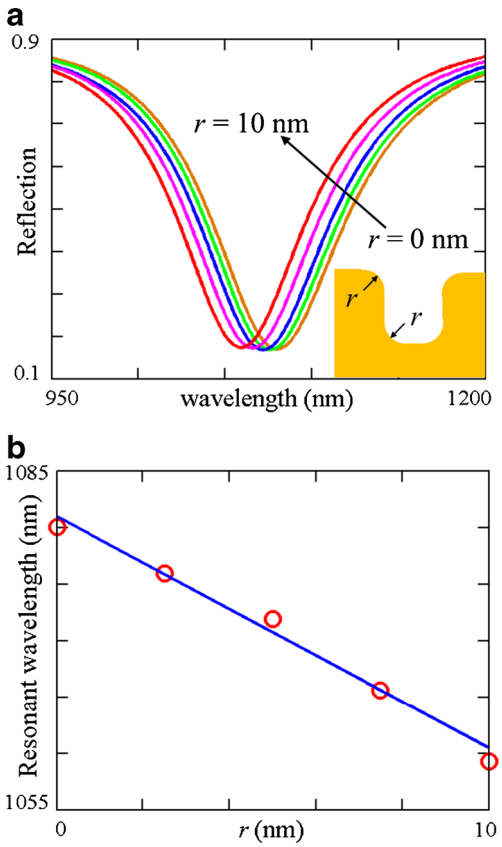


**Fig. 12** **a** Resonant wavelength changes as radius of round corner changes. Inset shows the rounded corner with radius of $r$. **b** Resonant wavelength versus radius when $\Lambda = 560$ nm, $w = 60$ nm, $d = 90$ nm, and $t = 800$ nm

on resonant wavelength, and we find that the resonant wavelength oscillates as the thickness of the dielectric medium increases. The reason is that the dielectric medium above the grooves form a cavity, and increasing the thickness of the dielectric medium causes the waves in the dielectric layer to change between constructive interference and destructive interference. We find in the structure that the minimum amplitude of oscillation in the resonant wavelength is less than 5 nm. The physical reason comes from the minimum reflection in the nanograting structure, so the cavity effect in the dielectric layer is small. A plasmonic sensor with small oscillations in the resonant wavelength as the thickness of the dielectric medium changes is preferred in order to reduce the measurement error due to an uncertain thickness of the dielectric medium. This device has good sensitivity and FOM values compared to other plasmonic sensors. Finally, we study the effect of rounded corners. We find that the rounded corners with a small radius of $r$ effectively reduce the nanogroove depth by about $0.2r$. These results will lead to a better understanding of the accuracy of plasmonic sensors covered by dielectric media.

**Acknowledgments** This research was supported in part by a Baylor ECS research initiation grant.

## References


1. Jiří H, Sinclair SY, Gnter G (1999) Surface plasmon resonance sensors: review. Sens Actuators B 54(1–2):3–15
2. William LB, Alain D, Thomas WE (2003) Surface plasmon subwavelength optics. Nature 424:824–830
3. Ekmel O (2006) Plasmonics: merging photonics and electronics at nanoscale dimensions. Science 311:189–193
4. Wen DL, Fei D, Jonathan H, Stephen YC (2011) Three dimensional cavity nanoantenna coupled plasmonic nanodots for ultrahigh and uniform surface-enhanced Raman scattering over large area. Opt Express 19(5):3925–3936
5. Jeffrey NA, Paige Hall W, Olga L, Nilam CS, Jing Z, Richard P, Van D (2008) Biosensing with plasmonic nanosensors. Nat Mater 7:442–453
6. Alexandre GB (2012) Plasmonics for future biosensors. Nat Photon 6:709–713
7. Ian MW, Xudong F (2008) On the performance quantification of resonant refractive index sensors. Opt Express 16(2):1020–1028
8. Lin W, Xiaodong Z, Ping B (2014) Plasmonic metals for nanohole-array surface plasmon field-enhanced fluorescence spectroscopy biosensing. Plasmonics 9:825–833
9. Tiffany H, Xueli L, Jonathan H (2013) Plasmonic grating nanostructure to detect refractive index. In: Frontiers in Optics. paper FTh2D, Orlando
10. Gordon II JG, Ernst S (1980) Surface plasmons as a probe of the electrochemical interface. Surface Sci 101(1–3):49–506
11. Claes N, Bo L, Tommy L (1982) Gas detection by means of surface plasmon resonance. Sens Actuators 3:79–88
12. Kahl M, Voges E (2000) Analysis of plasmon resonance and surface-enhanced Raman scattering on periodic silver structures. Phys Rev B 61:14078–14088
13. Francisco L, Ignacio T, Mario MJ (2010) Light intensity enhancement inside the grooves of metallic gratings. J Opt Soc Am B 27(10):1998–2006
14. López-Ríos T, Wirgin A (1984) Role of waveguide and surface plasmon resonances in surface-enhanced Raman scattering at coldly evaporated metallic films. Solid State Commun 52(2):197–201
15. Wirgin A, Maradudin AA (1985) Resonant enhancement of the electric field in the grooves of bare metallic gratings exposed to S-polarized light. Phys Rev B 31:5573–5576
16. Wirgin A, Maradudin AA (1986) Resonant response of a bare metallic gratings to S-polarized light. Prog Surf Sci 22(1):1–99
17. García-Vidal FJ, Sánchez-Dehesa J, Dechelette A, Bustrarret E, Lpez-Ros T, Fournier T, Pannetier B (1999) Localized surface plasmons in lamellar metallic gratings. J Light wave Technol 17(11):2191–2195
18. Garca-Vidal FJ, Martín-Moreno L (2002) Transmission and focusing of light in one-dimensional periodically nanostructured metals. Phys Rev B 66:155412
19. López-Ríos T, Mendoza D, García-Vidal FJ, Snchez-Dehesa J, Pannetier B (1998) Surface shape resonances in lamellar metallic gratings. Phys Rev Lett 81:665–668
20. Lalanne P, Hugonin JP, Astilean S, Palamaru M, Möller KD (2000) One-mode model and Airy-like formulae for one-dimensional metallic gratings. J Opt A: Pure Appl Opt 2(1):48–51
21. Yilei L, Hugen Y, Damon BF, Xiang M, Wenjuan Z, Richard MO, Tony FH, Phaedon A (2014) Graphene plasmon enhanced vibrational sensing of surface-adsorbed layers. Nano Lett 14(3):1573–1577
22. Moharam MG, Grann EB, Pommet DA, Gaylord TK (1995) Formulation for stable and efficient implementation of the rigorous coupled-wave analysis of binary gratings. J Opt Soc Am A 12(5):1068–1076
23. Li XF, Yu SF (2010) Extremely high sensitive plasmonic refractive index sensors based on metallic grating. Plasmonics 5:389–394
24. Lifeng L (1996) Formulation and comparison of two recursive matrix algorithms for modeling layered diffraction gratings. J Opt Soc Am A 13(5):1024–1035
25. Palik ED (1985) Handbook of Optical Constants of Solids Part II. Academic
26. Patrice G, Jean-Philippe T, Evangelos G, Romain B, Mikhail AK, Marlan OS, Federico C (2010) Large enhancement of nonlinear optical phenomena by plasmonic nanocavity gratings. Nano Lett 10(12):4880–4883
27. Siwen Z, Haitao L, Guoguang M (2011) Electromagnetic enhancement by a periodic array of nanogrooves in a metallic substrate. J Opt Soc Am A 28(5):879–886
28. Maier SA (2007) Plasmonics: Fundamentals and Applications. Springer, New York
29. Likang C, Jing Z, Wenli B, Qing W, xin W, Guofeng S (2010) Spatial mode selection by the phase modulation of subwavelength plasmonic grating. Plasmonics 5:423–428
30. Alina K, Olga K, Mark A, Benny H, Aid G, Ibrahim A (2009) Theoretical and experimental investigation of enhanced transmission through periodic metal nanoslits for sensing in water environment. Plasmonics 4:281–292
31. Adam DM, Richard PVD (2003) Single silver nanoparticles as real-time optical sensors with zeptomole sensitivity. Nano Lett 3(8):1057–1062
32. Alexandre GB, Reuven G, Brian L, Karen LK (2004) Surface plasmon sensor based on the enhanced light transmission through arrays of nanoholes in gold films. Langmuir 20(12):4813–4815

33. Na L, Martin M, Tomas W, Mario H, Harald G (2003) Infrared perfect absorber and its application as plasmonic sensor. Nano Lett 10(7):2342–2348
34. Hyungsoon I, Si HL, Nathan JW, Timothy WJ, Nathan CL, Prashant N, David JN, Sang-Hyun Oh (2011) Template-stripped smooth Ag nanohole arrays with silica shells for surface plasmon resonance biosensing. ACS Nano 5(8):6244–6253
35. Antonine L, Hyungsoon I, Nathan CL, Sang-Hyun Oh (2007) Periodic nanohole arrays with shape-enhanced plasmon resonance as real-time biosensors. Appl Phys Lett 90:243110
36. Jian Y, Pol VD (2011) Improvement of figure of merit for gold nanobar array plasmonic sensors. Plasmonics 6:665–671
37. Yang S, Jianhua Z, Tianran L, Yuting T, Ruibin J, Mingxuan L, Guohui X, Jinhao Z, ZhangKai Z, Xuehua W, Chongjun J, Jianfang W (2013) Plasmonic gold mushroom arrays with refractive index sensing figures of merit approaching the theoretical limit. Nat Commun 4:2381
38. Lin P (2007) Spectral sensitivity of two-dimensional nanohole array surface plasmon polariton resonance sensor. Appl Phys Lett 91:123112
39. Imogen MP, Yousif AK, Koray A, Harry AA (2011) Compliant metamaterials for resonantly enhanced infrared absorption spectroscopy and refractive index sensing. ACS Nano 5(10):8167–8174
40. Jan B, Andreas T, Arpad J, Ulrich H, Carsten S (2010) The optimal aspect ratio of Gold nanorods for plasmonic bio-sensing. Plasmonics 5:161–167
41. Jianjun C, Zhi L, Yujiao Z, Zhongliang D, Jinghua X, Qihuang G (2013) Coupled-resonator-induced fano resonances for plasmonic sensing with ultra-high figure of merits. Plasmonics 8:1627–1631
42. Hyun CK, Xing C (2009) SERS-active substrate based on gap surface plasmon polaritons. Opt Express 17(20):17234–17241
43. Siwen Z, Haitao L, Guoguang M (2010) Electromagnetic enhancement by a single nano-groove in metallic substrate. J Opt Soc Am A 27(7):1555–1560